DOI: 10.3901/CJME.2015.1028.128, available online at www.springerlink.com; www.cjmenet.com

# Continuous Separation of Multiple Size Microparticles using Alternating Current Dielectrophoresis in Microfluidic Device with Acupuncture Needle Electrodes

TAO Ye[1], REN Yukun[1, 2, *], YAN Hui[1], and JIANG Hongyuan[1, *]

1 *School of Mechatronics Engineering, Harbin Institute of Technology, Harbin 150001, China*
2 *State Key Laboratory of Fluid Power Transmission and Control, Zhejiang University, Hangzhou 310027, China*

Received July 22, 2015; revised October 23, 2015; accepted October 28, 2015

**Abstract:** The need to continuously separate multiple microparticles is required for the recent development of lab-on-chip technology. Dielectrophoresis(DEP)-based separation device is extensively used in kinds of microfluidic applications. However, such conventional DEP-based device is relatively complicated and difficult for fabrication. A concise microfluidic device is presented for effective continuous separation of multiple size particle mixtures. A pair of acupuncture needle electrodes are creatively employed and embedded in a PDMS(poly-dimethylsiloxane) hurdle for generating non-uniform electric field thereby achieving a continuous DEP separation. The separation mechanism is that the incoming particle samples with different sizes experience different negative DEP(nDEP) forces and then they can be transported into different downstream outlets. The DEP characterizations of particles are calculated, and their trajectories are numerically predicted by considering the combined action of the incoming laminar flow and the nDEP force field for guiding the separation experiments. The device performance is verified by successfully separating a three-sized particle mixture, including polystyrene microspheres with diameters of 3 μm, 10 μm and 25 μm. The separation purity is below 70% when the flow rate ratio is less than 3.5 or more than 5.1, while the separation purity can be up to more than 90% when the flow rate ratio is between 3.5 and 5.1 and meanwhile ensure the voltage output falls in between 120 V and 150 V. Such simple DEP-based separation device has extensive applications in future microfluidic systems.

**Keywords:** continuous separation of multiple size particles, dielectrophoresis, acupuncture needle electrodes, microfluidic

## 1 Introduction

Dielectrophoresis(DEP) is a promising method that can be used to manipulate, transport and separate samples of particles and biological micro-objects such as bacteria and cancer cells from blood, which has a broad application prospects for medical diagnosis in hospitals and particle filtration of water quality monitoring[1–2]. The phenomenon of DEP originates from the interaction between the induced dipole moment of a polarizable particle suspended in a dispersing medium and the applied non-uniform electric field. The electric field polarizes the particle, if the polarizability of the particle is greater than the surround liquid, it experiences a positive DEP(pDEP) force that attracts it towards high field intensity region. The opposite circumstance gives rise to negative DEP(nDEP) force that repels particle away from region of high electric fields. Both nDEP and pDEP have been frequently applied to sort and separate micro- or nano- particles and various kinds of cells[3–7]. In order to generate DEP, it is necessary for a field gradient to be generated in microfluidic devices. Generally speaking, there are two popular methods to achieve this goal depending on a variety of chip design and fabrication. In the literature, the traditional method patterns a micro-electrode array embedded in the microchannel by photolithographic deposition of metallic materials[8–10]. However, DEP need not be always performed with metal electrodes. Non-uniform electric field can also be generated by using insulating structures immersed in a conducting electrolyte. As a result, another approach to induce DEP builds local constricted region with insulating structures or hurdles[2, 11–13].

Compared to the conducting electrode based DEP, the insulator based DEP(iDEP) provides several conspicuous advantages such as more convenient fabrication process, less contamination issues, chemical inert and so on[14–15]. Therefore, DC-iDEP devices have widely been utilized to separate binary particle samples either by size effect or by dielectric property difference[16–18]. LAPIZCO-ENCINAS, et al[19–20], employed 3D insulating post array to collect and separate live and dead bacteria. HAWKINS, et al[21], developed a continuous-flow DEP spectrometer system based on 3D iDEP technique using dc-biased ac electric fields.

* Corresponding author. E-mail: rykhit@hit.edu.cn; jhy_hit@sina.com
Supported by National Natural Science Foundation of China(Grant No. 51305106), Fundamental Research Funds for the Central Universities, China(Grant Nos. HIT. NSRIF. 2014058, HIT. IBRSEM. 201319), and Open Foundation of State Key Laboratory of Fluid Power Transmission and Control, China(GZKF-201402)

In essence, the DEP-based colloidal separation applications are not restricted to binary particle suspension, and they have even been successfully extended to separate much more complex particle mixtures such as multiple type of bacterial cells[22] or charged polymer particles with a H-filter[22–23]. To our scrutiny of the current references, however, separating multiple particle mixtures in a continuous flow by using iDEP technique with low voltages(less than 200 V(voltage peak to peak)) has not yet been reported. On the contrary, as for applying high voltages, both the non-negligible Joule medium heating and the field-induced membrane stress of the cells are great challenges for the separation science.

Inspired by these previous findings, we introduce a simple iDEP microfluidic device with acupuncture needle electrodes for continuous separation of multiple size microparticle mixtures using negative AC DEP as shown in Fig. 1. In this device, voltages energized on the electrodes are less than 100 V, which implies less thermal effect influences the experimental results. The liquid flow inside the microchannel is driven by a hydraulic pressure difference, and the strong AC electric field gradient is confined within a small region around the PDMS hurdle. When the incoming particles move through the hurdle area, the negative DEP force can deviate the trajectories of these particles of different sizes that subsequently move into different downstream branches.

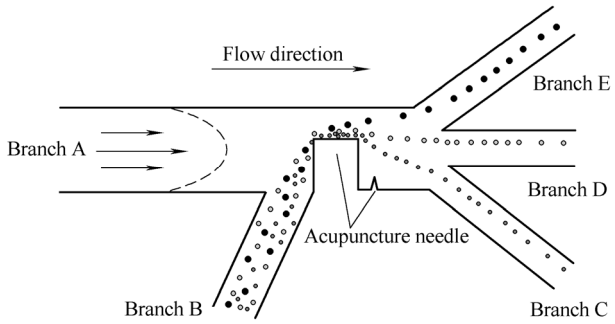


Fig. 1. Schematic illustration of the DEP separation device (not to scale)

Our device has several advantages as compared to previous DEP-based separation devices reported in the literature: (1) The usage of acupuncture needle electrodes facilitates the integration of working electrodes into PDMS microchannels so that the device assembly is simple; (2) The sidewall acupuncture needle electrodes generate 3D electric field throughout the entire channel hence exert stronger DEP force on particle samples; (3) The device is able to separate multiple size particles continuously by AC DEP in one step, while most of previous devices need multiple steps.

## 2 Materials and Methods

### 2.1 Theory of dielectrophoresis

For a homogeneous spherical particle of radius R, the net time-averaged DEP force in a harmonic AC electric field $\boldsymbol{E}(t)=\mathrm{Re}\left(\widetilde{\boldsymbol{E}}\mathrm{e}^{\mathrm{j}\omega t}\right)$ can be obtained by the point dipole approximation[24–25]:

$$\left\langle \boldsymbol{F}_{\mathbf{DEP}} \right\rangle = \pi\varepsilon_{\mathrm{f}} R^3 \,\mathrm{Re}\left(f_{\mathrm{CM}}(\omega)\right)\nabla\left(\widetilde{\boldsymbol{E}}\bullet\widetilde{\boldsymbol{E}}^{*}\right), \qquad (1)$$

where $\mathrm{Re}(\cdots)$ is the real part of a complex number, and * denotes the complex conjugate operator. $f_{\mathrm{CM}}(\omega)$ is the well-known Clausius–Mossotti (CM) factor, and depends on the angular frequency $\omega=2\pi f$ of the applied sinusoidal voltage:

$$f_{\mathrm{CM}}(\omega)=\frac{\tilde{\varepsilon}_{\mathrm{p}}-\tilde{\varepsilon}_{\mathrm{f}}}{\tilde{\varepsilon}_{\mathrm{p}}+2\tilde{\varepsilon}_{\mathrm{f}}}, \qquad (2)$$

$$\tilde{\varepsilon}_{\mathrm{p,f}}=\varepsilon_{\mathrm{p,f}}-\mathrm{j}\frac{\sigma_{\mathrm{p,f}}}{\omega}, \qquad (3)$$

where subscripts p and f represent particle and the suspending medium, respectively. The $\tilde{\varepsilon}_{\mathrm{p}}$ and $\tilde{\varepsilon}_{\mathrm{f}}$ are the complex permittivity of colloidal particle and fluid, respectively. $\varepsilon$ and $\sigma$ denote the real permittivity and electrical conductivity of the corresponding dielectric material, and $j$ is the imaginary unit. For a spherical particle, the in-phase component (real part) of the polarization (CM) factor ranges from $-0.5$ to 1 and defines the sign of DEP force, which is either positive when particles are attracted toward high field intensity regions(pDEP) or negative when particles are repelled away from areas of high electric fields(nDEP).

It is quite clear that in the high frequency limit (i.e. $\omega\to\infty$), the CM factor is mainly determined by the dielectric permittivity of both the particle and suspending medium. In contrast, in DC limit ($\omega\to 0$) the CM factor mainly depends on the conductivities of the particle and liquid medium.

Since they are of a net surface charge density, polystyrene(PS) particles at nano- and micro-meter scale do not behave as ideal insulators. An equivalent bulk conductivity of the latex particles is related to the surface conductance $K_{\mathrm{s}}$ through[26–27]

$$\sigma_{\mathrm{p}}=2K_{\mathrm{s}}/r. \qquad (4)$$

Since the diameter of all the particle samples involved is more than 1μm, the surface conductance $Ks$ used in present work is about 1.2 nS[28–29]. From Eq. (4), this equivalent bulk conductivity of latex particles is a decreasing function of particle diameter, which causes a decrease in the low-frequency conductivity plateau of the CM function with increasing radius as shown in Fig. 2(a).

Fig. 2(a) shows the in-phase component of CM factor as a function of field frequency for colloidal PS particles suspended in DI water (1.5 μS/cm). When the field frequency is beyond 1 MHz, the real part of all the CM functions is approaching –0.5, indicating that all the latex particles experience nDEP forces in this frequency range. From Fig. 2(b), the short-range nDEP force repels the particles away from both the insulating hurdle and the conducting electrode, and therefore changes their trajectories. However, the magnitude of nDEP force is proportional to $R^3$ based on Eq. (1), which means that all the sample particles are governed by obvious different DEP force thereby resulting in different motion trajectory for separation.

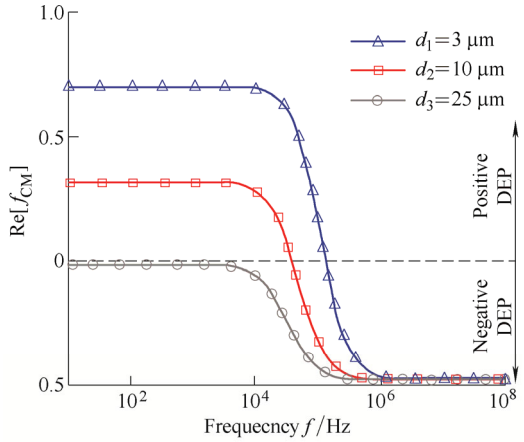


(a) CM factor as a function of electric field frequency

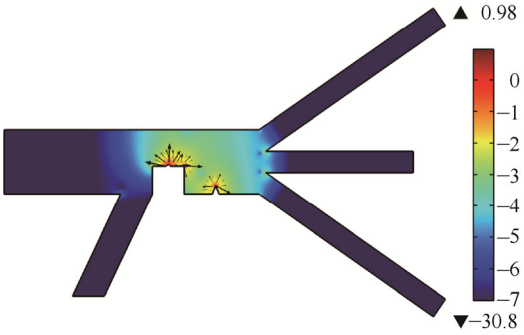


(b) Surface and arrow plot of nDEP induced particle velocity

Fig. 2. DEP force resulting in different motion trajectory for particles separation

## 2.2 Particle trajectory prediction

In typical microsystems, the inertial effect can be safely dropped, so the particle velocity $\boldsymbol{v}_{\mathrm{p}}$ can be treated as the direct measure of the surrounding flow velocity $\boldsymbol{u}_{\mathrm{f}}$ plus the velocity induced by the external force $\langle \boldsymbol{F}_{\mathrm{DEP}} \rangle$ acting on the particle,

$$\boldsymbol{v}_{\mathrm{p}} = \boldsymbol{u}_{\mathrm{f}} + \frac{\langle \boldsymbol{F}_{\mathrm{DEP}} \rangle}{6\pi\eta R} = \boldsymbol{u}_{\mathrm{f}} + \frac{\varepsilon_{\mathrm{f}} R^2 \,\mathrm{Re}\left(f_{\mathrm{CM}}(\omega)\right) \nabla\left(\widetilde{\boldsymbol{E}} \cdot \widetilde{\boldsymbol{E}}^*\right)}{6\eta}. \tag{5}$$

We can express above equation in a more explicit form:

$$v_{\mathrm{p}\_x} = u_{\mathrm{f}\_x} + \frac{\varepsilon_{\mathrm{f}} R^2 \,\mathrm{Re}\left(f_{\mathrm{CM}}(\omega)\right)}{6\eta} \frac{d\left(\widetilde{\boldsymbol{E}} \cdot \widetilde{\boldsymbol{E}}^*\right)}{\mathrm{d}x}, \tag{6a}$$

$$v_{\mathrm{p}\_y} = u_{\mathrm{f}\_y} + \frac{\varepsilon_{\mathrm{f}} R^2 \,\mathrm{Re}\left(f_{\mathrm{CM}}(\omega)\right)}{6\eta} \frac{d\left(\widetilde{\boldsymbol{E}} \cdot \widetilde{\boldsymbol{E}}^*\right)}{\mathrm{d}y}. \tag{6b}$$

Finally, the particle position $\boldsymbol{x}_{\mathrm{p}}(t)$ at any time instant can be determined by making an integral of the particle velocity:

$$\boldsymbol{x}_{\mathrm{p}}(t) = \boldsymbol{x}_0 + \int_0^t \boldsymbol{v}_{\mathrm{p}}(\tau)\,\mathrm{d}\tau, \tag{7}$$

where $\boldsymbol{x}_0$ is the particle initial position.

## 2.3 Numerical simulation

The Laplace Equation $\nabla^2 \tilde{\phi} = 0$ is solved to obtain the bulk potential $\tilde{\phi}$ and the electric field $\widetilde{\boldsymbol{E}} = -\nabla\tilde{\phi}$, subjected to $\tilde{\phi} = A$ ($A$ is the voltage amplitude applied) and $\tilde{\phi} = 0$ on the electrode pair, respectively, with other channel walls treated as insulating boundaries $\boldsymbol{n} \cdot \tilde{\phi} = 0$.

The Stokes Equation is solved to obtain the flow velocity $\boldsymbol{u}_{\mathrm{f}}$, with fixed inflow velocity at inlet channel A and B. Zero pressure is applied at the outlet channel C, D and E, and all the channel sidewalls are treated as no-slip wall boundaries. Once the electric field $\widetilde{\boldsymbol{E}}$ and flow velocity $\boldsymbol{u}_{\mathrm{f}}$ are known, Eq. (6) and Eq. (7) are solved in sequence to acquire the particle motion trajectory.

## 2.4 Chip fabrication and system setup

The fabrication of the microfluidic chip follows basic soft lithography process, and the distance between the electrode pair is adjusted by hand under microscope. In brief, two 30 μm thick photoresist layers were patterned on a clean glass slide, and after UV exposure, the photoresist was developed to create mold and cavities for housing acupuncture needle electrodes(*Hanyi, Beijing Hanyi Medical Instruments Centre*). The electrodes were fixed by a pair of magnetic patch on the back of the glass slide and distance of the electrodes was adjusted by hand under microscope. PDMS gel was poured on the mold and cured. After curing PDMS with embedded acupuncture needle electrodes, the channel was punched to create five reservoirs and then bonded with a glass substrate using oxygen plasma treatment.

The device is shown in Fig. 3, which consists of a 300 μm wide and 1400 μm long main channel with five branch channels that end up in two upstream inlets (A and B) and three downstream outlets (C, D and E). The widths of

branch channels A, B, C, D and E are 300 μm, 150 μm, 100 μm, 100 μm, and 100 μm, respectively. Moreover, the distance of the two needle tips is about 300 μm. All channels are near 50 μm deep (the thickness of the photoresist was reduced by patterning). All five reservoirs at the inlets and outlets are the same, and each has 5 mm in height and 6 mm in diameter, giving rise to volumetric capacity of about 141 μL. Such large reservoir volume was found to be able to generate steady flow more than 10 min via controlling the liquid level difference.

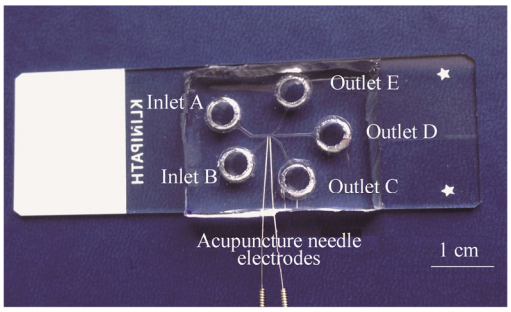


(a) PDMS microchip with acupuncture needle electrodes

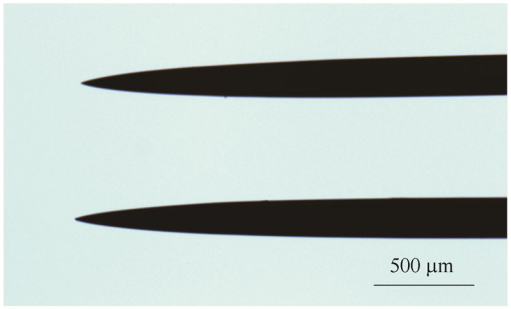


(b) Micrograph of acupuncture needle electrodes

Fig. 3. Design of the microchip for separation

Latex particles(Sigma) with the diameter of 3 μm, 10 μm and 25 μm are suspended in DI water with the conductivity of 1.5 μS/cm for DEP experiments. The sample number ratios are set to be 20 (3 μm):6 (10 μm):1 (25 μm). The particle mixtures are dispersed three times by ultrasonic cleaner before experiments.

The DEP forces induced by the acupuncture needle electrodes were generated by ac voltages energized by a function generator (TGA12104, TTi), and amplified by an amplifier (Model2350, TEGAM). The particle motion was monitored by an optical microscope (BX53, Olympus) and video-taped by a CCD camera (RETIGA2000R, Qimaging).

## 3 Results and Discussions

In order to suppress both the induced double-layer charging effect and AC electroosmotic flow[27, 30], we choose field frequencies more than 1MHz in our experiments. On the basis of the prediction that latex particles of different diameters possess distinct DEP responses in this frequency range, we used the microfluidic device to separate a mixture of latex particles with diameters of 3 μm, 10 μm and 25 μm. For experiments where three types of particles were separated, the separation purity was expressed as

$$\eta = \left(1 - \frac{N_{\text{loss}}}{N_A}\right) \times 100\% , \tag{8}$$

where $N_A$ is the total number of particles (counted per half minute) moving into a downstream outlet, and $N_{\text{loss}}$ is the number of unexpected samples. For instance, the outlet E is the theoretical path of the particle of 25 μm in diameter, so if there are some particles with other sizes, the separation purity can be calculated using Eq. (8). Moreover, in our experiments the steady flow can last at least 10 minutes because of the large reservoir volume, so we have a steady flow velocity near to be 1200 μm/s in the mainchannel (inlet A). For analyzing the flow effect on the separation purity, we adjusted the flow velocity in the inlet B, and defined a parameter $\gamma$ to describe the flow velocity ratio between inlet A and inlet B.

### 3.1 Effect of energized voltage

To achieve the continuous separation of multiple size particles, it is important to identify the threshold voltage required for pushing the 25 μm particles to the upper branch E, but still keeping the 10 μm and 3 μm particles to the middle branch D and lower branch C, respectively. Fig. 4 shows a comparison of the superposed particle trajectories under different voltages with a flow velocity ratio of 4.2. It is indicated that the magnitude of trajectory deviation for both larger and smaller particles increases with increasing the voltage level. This is because the DEP force is proportional to the gradient of the electric-field intensity, $\nabla E^2$. The experimental results show that when the energized peak to peak voltage is below 112.5 V, the purities of branch D, and branch C are both less than 70%, while the value for branch E is near 100% (Figs. 4(a), (b)). In contrast, if the voltage is larger than 150 V, the purities of branch E, and branch D are both less than 70%, but the branch C is close to 100% (Figs. 4(c), (d)). Therefore, the experiments indicate that if we fix the flow rate ratio to 4. 2, a probable energized voltage region is from 120 V to 150 V for keeping the purities of all the three branches with a level of more than 90%.

### 3.2 Effect of flow rate ratio

Flow rate ratio, $\gamma$, is another important factor required for a microfluidic device to operate its separation functions. As the flow rate in the main channel is fixed in our experiments, the fluid flow rate in inlet B is a variable parameter. By increasing $\gamma$, although sample throughput can be enhanced, the force action time is decreased, thereby a larger DEP force is required to account for this increased sample transport velocity. The proper conditions for

matching hydrodynamic drag force and DEP force must meet. Fig. 5 shows the effect of $\gamma$ on sorting of multiple particles. As Figs. 5(a), (b) shows, when the $\gamma$ is relative high the samples are squeezed closely to the hurdle edge, and pass fast through the hurdle, resulting in a very short DEP action time. Therefore, the particles are all pushed into the lower branches. In contrast, if $\gamma$ is relative low, although the incoming samples can be raised up into upper branches, the separation purity is unsatisfactory as shown in Figs. 5 (c)(d).

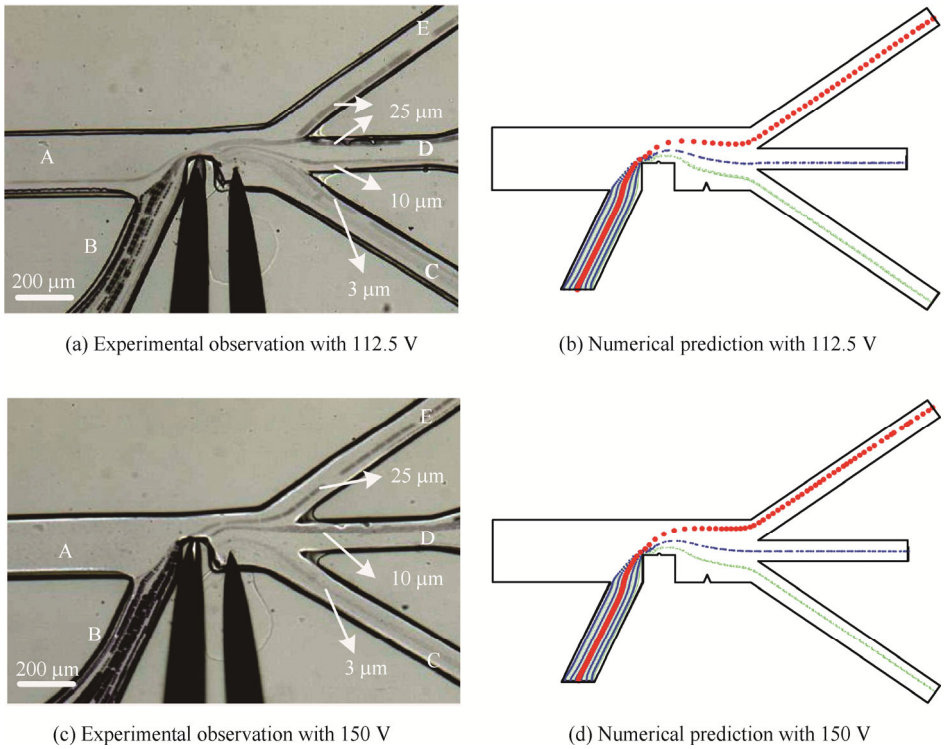


(a) Experimental observation with 112.5 V (b) Numerical prediction with 112.5 V

(c) Experimental observation with 150 V (d) Numerical prediction with 150 V

Fig. 4. Particle trajectories under different voltage outputs

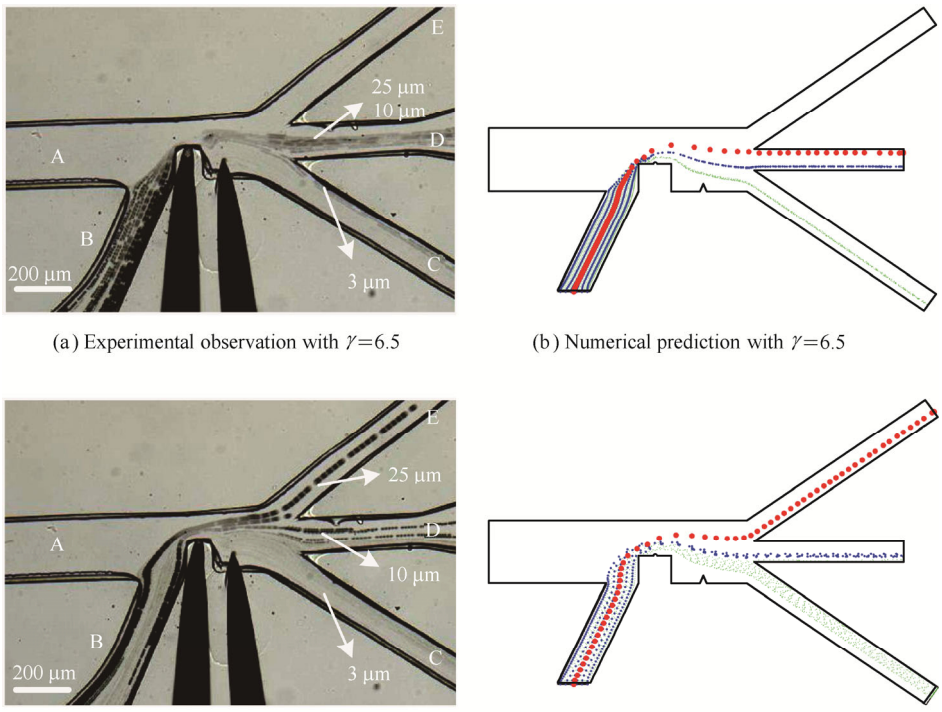


(a) Experimental observation with $\gamma$=6.5 (b) Numerical prediction with $\gamma$=6.5

(c) Experimental observation with $\gamma$=1.2 (d) Numerical prediction with $\gamma$=1.2

Fig. 5. Particle trajectories under different flow rate ratio

In our practical experiments, purity of outlet D is the most difficult to achieve, so it can be used as an evaluation criterion for this separation device. The values of $\gamma$ and voltages for keeping the purity of outlet D on a high level (>90%) are shown in Table 1. The ideal flow rate ratio that ensures a good separation purity is $3.5<\gamma<5.1$. In this

region, the voltage output (120 V$<V_{pp}<$150 V) is proportional to the flow rate ratio for keeping a good purity in outlet D. When the flow rates ratio is lower than the minimum value or larger than the maximum ratio, we cannot obtain a good purity no matter how to adjust the voltage output.

**Table 1. Purity in outlet D associated with flow rate ratio and voltage output**

| Flow rate ratio $\gamma$ | Voltage output $V_{pp}$/V | Purity in outlet D $\eta$ |
|---|---|---|
| <3.5 | | <70% |
| 3.5−5.1 | 120−150 | >90% |
| >5.1 | | <70% |

### 3.3 Typical case and possible joule heating effect

As discussed previously, the magnitude of the particle trajectory deviation is proportional to the DEP force acting on the particle, and hence the particle volume. Therefore, the trajectories of the particles of different sizes can be diverted to different streams after they pass the hurdle. A typical case of separation of the particles mixture is shown in Fig. 6(a) (voltage of 150 V, frequency of 1 MHz and fluid flow velocity ratio $\gamma$ is 4.2 ), which is obtained by superimposing a series of consecutive images of the moving particles. At first, the incoming particle mixture comes out as a single stream from the inlet branch channel B. Then the main stream of the buffer solution from inlet branch channel A squeezes the mixture and forces the particles to move closely to the hurdle. After the particles pass through the hurdle, their trajectories are changed. The trajectory deviation for a larger particle is greater than that for a smaller particle because of the different magnitude of the DEP force they experience at the hurdle. Thus, the single mixture stream is separated into three individual streams. Therefore, particles with different diameter move into different outlets (25 μm to E, 10 μm to D, 3 μm to C) by adjusting the voltage and inflow velocity. Numerical prediction on the trajectories of the incoming particle samples (Fig. 6(b)) shows a qualitative agreement with the experimental observation.

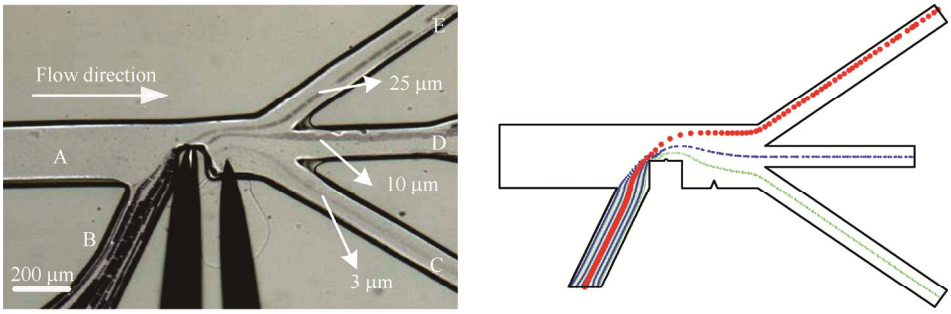


(a) Experimental observation of a typical case

(b) Numerical prediction of a typical case

Fig. 6. Trajectories of particles with 3 μm (green), 10 μm (blue) and 25 μm (red) diameter, respectively, under the combined action of the incoming laminar flow and nDEP force field.

Furthermore, as we know that under application of electric field in a microchannel, Joule heating appears because of the passage of electrical current through an electrolyte medium, and thus such heat results in temperature rise. As the electrical conductivity and permittivity are temperature-dependent properties of the electrolyte solution, the temperature rise can lead to changes in these fluid properties which in turn generate an electrothermal body force thereby to drive the fluid near the electrodes in a rotational manner[31]. Therefore, in the iDEP based devices, the electrothermal induced flow is undesirable. However, in our experiments there is not obvious joule heating effects. The possible reason is that although the applied electric field amplitude is 2500 V/cm, while the medium conductivity is only 1.5 μS/cm, so electric heat generation ($\frac{1}{2}\sigma|\mathrm{E}|^2$) is about 4.69 MW/m$^3$, which induces negligibly small local temperature rise, implying negligible Joule heating effects[32]. Moreover, as the concentration of the particles in the mixture is not heavy, we neglect any particle-particle interactions.

## 4 Conclusions

(1) The use of acupuncture needle electrodes facilitates the integration of working electrodes into PDMS microchannels so that the microfluidic separation device is simple.

(2) Under reasonable structure settings, the design in this work can effectively neglect joule heating hurt on bioparticles.

(3) In this design, the ideal flow rate ratio that ensures a good separation purity is 3.5$<\gamma<$5.1, and the related voltage output should be 120 V$<V_{pp}<$150 V to match the flow rate ratio.

(4) This work suggests the potential of integrating the present device with other microfluidic components into a lab-on-chip platform for chemical analysis and biomedical diagnosis.

## References


[1] PETHIG R. Review article-dielectrophoresis: status of the theory, technology, and applications[J]. *Biomicrofluidics*, 2010, 4(2): 022811–022846.

[2] REN Y, WU H, FENG G, et al. Effects of chip geometries on dielectrophoresis and electrorotation investigation[J]. *Chinese Journal of Mechanical Engineering*, 2014, 27(1): 103–113.

[3] SUSCILLON C, VELEV O D, SLAVEYKOVA V I. Alternating current-dielectrophoresis driven on-chip collection and chaining of green microalgae in freshwaters[J]. *Biomicrofluidics*, 2013, 7(2): 024109–024124.

[4] OTTO S, KALETTA U, BIER F, et al. Dielectrophoretic immobilisation of antibodies on microelectrode arrays[J]. *Lab on a Chip*, 2013, 14(5): 998–1012.

[5] REN Y, AO H, GU J. Research of micro-particle manipulation in micro systems using DEP force[J]. *Acta Phys Sin*, 2009, 58(11): 7.

[6] JIANG Hongyuan, REN Yukun, TAO Ye. Microwire formation based on dielectrophoresis of electroless gold plated polystyrene microspheres[J]. *Chinese Physics B*, 2011, 20(5): 057701–057709.

[7] DASH S, MOHANTY S. Dielectrophoretic separation of micron and sub-micron particles: a review[J]. *Electrophoresis*, 2014, 35(18): 2656–2672.

[8] LI M, QU Y, DONG Z, et al. Limitations of Au particle nanoassembly using dielectrophoretic force—a parametric experimental and theoretical study[J]. *Nanotechnology, IEEE Transactions on*, 2008, 7(4): 477–486.

[9] ABDALLAH B G, CHAO T C, KUPITZ C, et al. Dielectrophoretic sorting of membrane protein nanocrystals[J]. *ACS Nano*, 2013, 7(10): 9129–9137.

[10] LUMSDON S O, KALER E W, WILLIAMS J P, et al. Dielectrophoretic assembly of oriented and switchable two-dimensional photonic crystals[J]. *Applied Physics Letters*, 2003, 82(6): 949–951.

[11] KANG Y, CETIN B, WU Z, et al. Continuous particle separation with localized AC-dielectrophoresis using embedded electrodes and an insulating hurdle[J]. *Electrochimica Acta*, 2009, 54(6): 1715–1735.

[12] WANG L, FLANAGAN L A, MONUKI E, et al. Dielectrophoresis switching with vertical sidewall electrodes for microfluidic flow cytometry[J]. *Lab on a Chip*, 2007, 7(9): 1114–1134.

[13] YE J, YANG J, ZHENG J, et al. Rarefaction and temperature gradient effect on the performance of the Knudsen pump[J]. *Chinese Journal of Mechanical Engineering*, 2012, 25(4): 745–797.

[14] LI M, LI S, LI W, et al. Continuous particle manipulation and separation in a hurdle-combined curved microchannel using DC dielectrophoresis[J]. *AIP Conference Proceedings*, 2013, 1542: 1150–1153.

[15] ZHU J, CANTER R C, KETEN G, et al. Continuous-flow particle and cell separations in a serpentine microchannel via curvature-induced dielectrophoresis[J]. *Microfluidics and Nanofluidics*, 2011, 11(6): 743–795.

[16] LI M, LI S, CAO W, et al. Continuous particle focusing in a waved microchannel using negative dc dielectrophoresis[J]. *Journal of Micromechanics and Microengineering*, 2012, 22(9): 095001–095009.

[17] JEN C P, MASLOV N A, SHIH H Y, et al. Particle focusing in a contactless dielectrophoretic microfluidic chip with insulating structures[J]. *Microsystem Technologies*, 2012, 18(11): 1879–1965.

[18] REN Y, LI B, JIANG H. Control of the dielectric microrods rotation in liquid by alternating current electric field[J]. *Chinese Journal of Mechanical Engineering*, 2014, 27(3): 622–629.

[19] LAPIZCO-ENCINAS B H, SIMMONS B A, CUMMINGS E B, et al. Dielectrophoretic concentration and separation of live and dead bacteria in an array of insulators[J]. *Analytical Chemistry*, 2004, 76(6): 1571–1579.

[20] LAPIZCO-ENCINAS B H, SIMMONS B A, CUMMINGS E B, et al. Insulator-based dielectrophoresis for the selective concentration and separation of live bacteria in water[J]. *Electrophoresis*, 2004, 25(10–11): 1695–1704.

[21] HAWKINS B G, SMITH A E, SYED Y A, et al. Continuous-flow particle separation by 3D insulative dielectrophoresis using coherently shaped, dc-biased, ac electric fields[J]. *Analytical Chemistry*, 2007, 79(19): 7291–7300.

[22] KIM U, QIAN J, KENRICK S A, et al. Multitarget dielectrophoresis activated cell sorter[J]. *Analytical chemistry*, 2008, 80(22): 8656– 8707.

[23] LEWPIRIYAWONG N, YANG C. Continuous separation of multiple particles by negative and positive dielectrophoresis in a modified H-filter[J]. *Electrophoresis*, 2014, 35(5): 714–734.

[24] RAMOS A, MORGAN H, GREEN N G, et al. Ac electrokinetics: a review of forces in microelectrode structures[J]. *Journal of Physics D: Applied Physics*, 1998, 31(18): 2338–2353.

[25] JONES T B, JONES T B. *Electromechanics of particles*[M]. Cambridge University Press, 2005.

[26] ERMOLINA I, MORGAN H. The electrokinetic properties of latex particles: comparison of electrophoresis and dielectrophoresis[J]. *J Colloid Interface Sci*, 2005, 285(1): 419–448.

[27] RAMOS A, MORGAN H, GREEN N G, et al. AC electric-field-induced fluid flow in microelectrodes[J]. *Journal of Colloid and Interface Science*, 1999, 217(2): 420–422.

[28] ARNOLD W, SCHWAN H, ZIMMERMANN U. Surface conductance and other properties of latex particles measured by electrorotation[J]. *Journal of Physical Chemistry*, 1987, 91(19): 5093–5101.

[29] LEWPIRIYAWONG N, YANG C. AC-dielectrophoretic characterization and separation of submicron and micron particles using sidewall AgPDMS electrodes[J]. *Biomicrofluidics*, 2012, 6(1): 12807–12809.

[30] RAMOS A. *Electrohydrodynamic pumping in microsystems*[M]. Springer, 2011.

[31] GREEN N G, RAMOS A, GONZÁLEZ A, et al. Electrothermally induced fluid flow on microelectrodes[J]. *Journal of Electrostatics*, 2001, 53(2): 71–87.

[32] SRIDHARAN S, ZHU J, HU G, et al. Joule heating effects on electroosmotic flow in insulator-based dielectrophoresis[J]. *Electrophoresis*, 2011, 32(17): 2274–2355.


## Biographical notes


TAO Ye, born in 1985, is currently a PhD candidate at *School of Mechatronics Engineering, Harbin Institute of Technology, China* His interest topic is microfluidics and nanofluidics.
E-mail: tarahit@gmail.com

REN Yukun, born in 1981, is currently an associate professor at *School of Mechatronics Engineering, Harbin Institute of Technology, China.* His main research interests include microfluidics, AC electrokinetics, et al.
Tel: +86-451-86418028; Email:rykhit@hit.edu.cn

YAN Hui, born in 1974, is currently an associate professor at *School of Mechatronics Engineering, Harbin Institute of Technology, China.* His main research interests include metal rubber, microfluidics, et al.
E-mail: yanhui@hit.edu.cn

JIANG Hongyuan, born in 1960, is currently a professor and a PhD candidate supervisor at *School of Mechatronics Engineering, Harbin Institute of Technology, China.* His main research interests include metal rubber, microfluidics, et al.
E-mail: jhy_hit@sina.com